Semiannual Progress Report
NASA Grant NAG2-545
Astrometry with the ATF

1990 February 1 - 1990 July 31

Prepared for
NASA-Ames Research Center
Moffett Field, CA 94035

University of Texas at Austin
Department of Astronomy
Austin, Texas 78712

August 1990

William H. Jefferys
Principal Investigator

During the period covered by this report, Professor Matzner did a detailed study of the effects of gravitational radiation on the relative positions of objects, with the hope that astrometric detection of gravitational radiation might be possible. His report is attached. The results are discouraging. It would appear that narrow-field instruments in the ATF class are still several orders of magnitude less accurate than would be required for this very delicate kind of measurement.

However, the situation changes considerably when wide-field instruments are considered. An instrument such as POINTS ought to be able to detect gravitational radiation at this level with ease.

The list of bright quasars has been augmented. Of particular interest is the finding of quasars near two open clusters and one planetary nebula. These would be useful in determining absolute parallaxes of these objects. The report of the graduate student who did this work is also attached.

GRAVITATIONAL WAVE DETECTION

USING SPACE-BORNE OPTICAL INTERFEROMETERS

The possibility of detection of long-period gravitational radiation using a high-accuracy (10^{-5} arcsec), small-field (20 arcmin square) interferometer.

The propagation of photons from astronomical and cosmological sources follows null geodesics in the spacetime. Here we want to consider a flat space on which a propagating gravitational wave is superposed. The motion of a photon in the absence of the wave is described by a number of constants of its motion (essentially, the conserved components of its physical momentum). In the presence of the gravitational wave, there are fewer, but still enough of, conserved momenta to solve for the photon orbit. However, the presence of the gravitational wave modifies the relationship of the conserved momenta to the physical direction of propagation. This can lead to deviation of pointing or to a displacement of the image in the image plane.

Figure 1 shows a situation in which a net shift across the focal plane of the instrument will occur. The deflection of the target object is a function of the angle to the object referenced to the gravitational wave propagation direction, so objects separated by $\delta\theta$ in the image field will experience different deflections. However, the relative motion between two images is of order $\alpha h_+(\delta\theta)^2$, where h_+ is the amplitude of the gravitational wave, α depends on the geometry and is typically small (see below), and $\delta\theta \gtrsim 20$ arcmin $\gtrsim 5 \times 10^{-3}$ (the field of view), so there is a strong suppression of the observability of the wave-induced deflection.

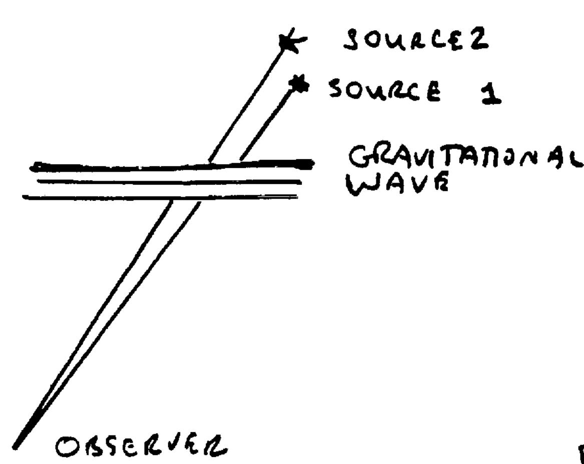

FIG 1

Figure 2 shows a possibility more appropriate to observing a real effect.

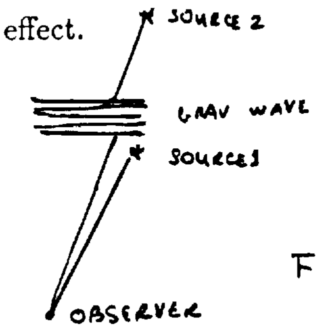

FIG ..

Here, only the direction to the more distant source is deflected. The amount of deflection is then of order αh_+, where again α depends on the geometry and h_+ is the amplitude of the wave. We now carry out the analysis and estimate angular deflection for various geometrical situations.

For a plane wave travelling at the z-direction, let

$$u = z - t,$$
$$v = z + t.$$

Then,

$$du\,dv = -dt^2 + dz^2.$$

The metric for weak gravitational waves is

$$ds^2 = -du\,dv + [1 + h_{xx}(u)]\,dx^2 + [1 - h_{xx}(u)]\,dy^2. \tag{1}$$

This is a typical h_+ polarization pattern; the other $(h_\times)$-polarization pattern involves a term $h_{xy}(u)\,dx\,dy$ that can be removed by a redefinition [a rotation in the $(x$–$y)$-plane]. The amplitude of the gravitational wave is $h_+ \equiv h_{xx}$.

In such a situation, there are still enough conserved momenta for photons to completely solve for the photon motion. (These are *not* the physical momenta; see below.)

$$p_x = \text{const.}, \qquad p_y = \text{const.}, \tag{2}$$
$$p_v = \tfrac{1}{2}(p_z + p_t) = \text{const.} \tag{3}$$

If the gravitational wave were not present, p_z and p_t would be separately constant.

The other component (not constant) of the momentum can be solved for because the photon path is *null*

$$g^{\alpha\beta} p_\alpha p_\beta = 0.$$

To the accuracy required, using the inverse of the metric (1) expanded to first order in h, this is

$$(p_z + p_t)(p_z - p_t) + (1 - h_+) p_x^2 + (1 + h_+) p_y^2 = 0, \tag{4}$$

or

$$(p_z - p_t) = -\frac{(1 - h_+) p_x^2 + (1 + h_+) p_y^2}{p_z + p_t}. \tag{5}$$

The right side of this expression is constant except for the appearance of h. Using (3), we have, to lowest order in h_+,

$$p_z = \overset{b}{p}_z + \frac{1}{2} h_+ \frac{p_x^2 - p_y^2}{\overset{b}{p}_z + \overset{b}{p}_t} \tag{6}$$

with the superscript "b" meaning "background" values (i.e., the values when $h_+ = 0$). Because of the form of the metric, we have $p_z = |p| \cos\theta$ where θ is the physical direction of propagation. (Here θ is measured from the z-axis, the direction of propagation of the gravitaional wave.) Because of the wave, the physical direction of propagation changes, since p_z changes. From (6), we obtain the change in propagation angle θ:

$$\Delta\theta = \frac{h_+}{2} \frac{\sin\theta_b \cos 2\phi_b}{1 + \cos\theta_b}, \tag{7}$$

where $\tan\phi_b = \overset{b}{p}_y / \overset{b}{p}_x$.

There are also changes in the transverse (ϕ) direction. Although p_x and p_y are separately constant even in the presence of the wave, they are not the physical components. Instead, $p_x(\text{physical}) = 1/(1 + h_+)^{1/2} p_x$ and $p_y(\text{physical}) =$

$1/(1-h_+)^{1/2}p_y$, so that

$$\tan\phi = \frac{p_y(\text{physical})}{p_x(\text{physical})} = \sqrt{\frac{1+h_+}{1-h_+}}\left(\frac{\overset{b}{p}_y}{\overset{b}{p}_x}\right)$$

$$\approx (1+h_+)\,\frac{p_x}{p_y} = \tan\phi_b + h_+\,\tan\phi_b,$$

$$\text{so that}\quad \Delta\phi = h_+\left(\frac{\tan\phi_b}{1+\tan^2\phi_b}\right).$$

As anticipated, both expressions for the deflection angle are proportional to h. In both cases, however, note that this deflection angle is a deflection in the photon path as it travels. Only if the wave is at the detector on Earth can this directly amount to a change in viewing direction. [This would be a subset of the case (a) considered above, and it yields diffferential deflection proportional to $h_+(\Delta\theta)^2$, where $\Delta\theta$ is the angular offset between the two sources.]

To analyze the apparent deflection in case (b) above, first note that the photon direction is the same after as before the wave passage. It is only during wave passage that the physical propagation changes. Hence, the situation can be idealized as a refraction in a plane sheet of glass, as follows.

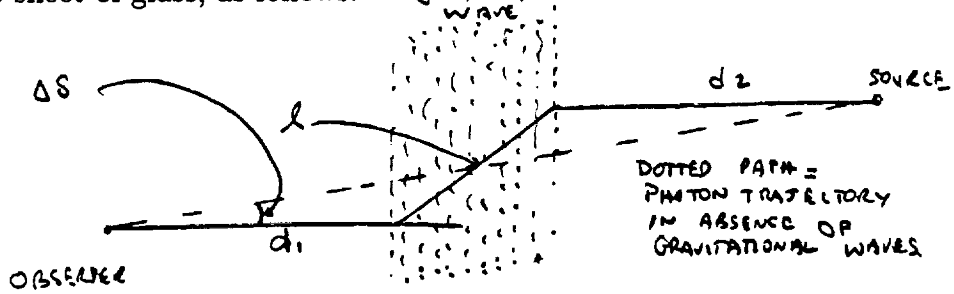

Gravitational deflection angle θ_g

Hence, as seen by the observer, the angular displacement of the source (compared to the no-wave case) is

$$\Delta\delta = \frac{\text{offset}}{d_1 + \ell\cos\theta_g + d_2} \approx \frac{\ell\theta_g}{d_1+d_2},$$

assuming that the total distance to the source is large compared to length of the region occupied by the wave.

Since the angle θ_g is of order h, the resulting offset in the viewing angle δ is of order

$$(\Delta\delta)_{\rm obs} \simeq \langle h \rangle \frac{\ell}{d},$$

where d is the distance to the optical source and ℓ is the duration of the gravitational wave pulse. In this expression we have dropped geometrical factors that are typically of order unity. We have also inserted the *average* value of h_+ throughout the wave; an oscillatory h_+ will have a much smaller deflection.

Because of the design of the space-borne optical interferometer, most sensitivity will be available for observed direction variations with period of order one year. A wave packet of ~ 1 light year scale in all directions (a single "positive-going" pulse with overall timescale ~ 1 year) is ideal.

Ideal detection geometry would thus comprise two sources—one fiducial, one for detection—as close to the Earth as possible to minimize d. Candidates might be a pair of white dwarf stars about ten light-years away and separated in distance by about one light-year. The suppression factor is then of order 1/10.

Estimates of the amplitude h_+ of the gravitational radiation can be made in several ways. A wave of period one year due to a binary star system (two 1/2 solar mass stars, separated by 1 AU) would have amplitude $h \sim 10^{-8}/r(\text{km})$ and so would be undetectable at any reasonable distance. A substantially relativistic collapse with a period of order one year would constitute a galaxy-mass collapse and is very improbable, but there is no clear single source candidate. Such a collapse would be detectable at 10^{-11} level from sources out to 300 Mpc. However, we can also imagine there is a stochastic background and estimate the amplitude of such a stochastic radiation field. A gravitational wave field has energy density proportional to $(\omega h_+)^2$:

$$\frac{\rho}{\rho_{\rm closure}} = \left(\frac{\omega}{2\pi/\text{yr.}}\right)^2 \left(\frac{h_+}{10^{-11}}\right)^2.$$

Thus, if $h_+ \simeq 10^{-11}$, then a uniform bath of *random* waves of period ~ 1 year would be sufficient to "close" the universe. With the estimate of $\alpha \sim 10^{-1}$ as the most favorable geometry, we would anticipate a maximum angular fluctuation $\sim 10^{-12}$ radians, $\sim 10^{-6}$ arcseconds. This would seem to be about one order of magnitude below the design sensitivity of the instrument.

The current observations of the millisecond pulsar give limits on the gravitational wave background in the ~ 1 year range. If we consider the recent report by J. Taylor as definitive, we find $\rho/\rho_{\text{closure}} \sim 10^{-4}$ (i.e., $h_+ \sim 10^{-13}$), which gives at least another 10^2 suppression on the detectability below the capability of the instrument. We should note, however, that any single source (e.g., the millisecond pulsar) sample waves in only one particular direction. The interferometer proposed will have the ability to observe in essentially any direction. Furthermore, the gravitational wave background can act as a noise source (diminishing with observations of more distant optical targets) most important for nearby stellar observations and should be considered in a signal-to-noise analysis.

More data search was conducted during this semester. Quasars known as variables were included, and we took a closer look especially at 3C 273 which is very bright and has a bright star nearby.
We also studied the list of Hipparcos' quasars and stars. We picked the bright ones and added them to our original list. We limit the list to 15.5 magnitude quasars. They are all confined in Table I.1.

From an object with magnitude m, photon flux can be calculated using the following relation *:

$$S = N t D^2 (\Delta\lambda) \, 10^{-0.4 m}$$

where:

$N = 10^4$ photons / (sec cm^2 nm) for a 0 magnitude A0 star at a wavelength of 550 nm.
t = transmittancy from the top of atmosphere to the detector (here we take to be unity)
D = diameter of the telescope (1.85×10^2 cm)
$\Delta\lambda$ = bandpass of the instrument used (400 nm).

Knowing thei required instrumental minimum of 10^8 photons, we can calculate the ideal integration time. The average total time will be obtained by multiplying the ideal integration time by 1160. Table I.2 explains total observation time calculation.

The reference stars are chosen within 10 arcminutes from each quasar with the requirement that those objects should be at least 2 arcsec apart. These reference stars are obtained from the Guide Star Catalog of Space Science Institute. A special computer program called "pickles data" then read and locate them around its quasar.

Two open clusters and one planetary nebulae which are which are close in position to our quasars or Hipparcos star are listed in Table II.

* Schroeder, D. J., Astronomical Optics, (Academic Press Inc., San Diego, 1987)

TABLE I.2

Random Errors

- Integration time needed to reach a given accuracy is increased by random errors.

	Error Source	F^*
1.	Photon Statisticces (σ_0)	1.000
2.	Background Light	.002
3.	Image Shape/Size	.30
4.	Image Motion (Jitter)	(a)
5.	Grating Imperfections	(a)
6.	Grating Motions	(b)
7.	Grating Alignment	TBD
8.	Field Modeling	0.060
9.	Reduction Algorithm	$\ll 1$
10.	Postfocal Response Variation	TBD
11.	Reference Star Errors	(c)
12.	Contamination	TBD
	TOTAL TIME FACTOR:	1.362 + TBD

$^*F$ = Contribution to the integration time enhancement factor; total time enhancement is the sum of the individual F's.

NOTES: (a) The design requirement corresponding to $F \ll 1$ is feasible.
(b) Included in jitter.
(c) With proper selection of fields and reference stars, this error will be negligible ($F \ll 1$).

TABLE 1.2 (Cont.)

Light Loss Effects

- Integration time needed to reach a given accuracy is increased by light and other information losses.

Source of Information Loss	Type of Loss	Throughput
A. Grating Rejection	Light	0.25
B. Mask for Grating Shadow	Light	0.75
C. Grating Intrinsic	Information	0.50
D. Loss in Optics	Light	0.50
E. Detector Quantum Inefficiency	Light	0.10
F. One-dimensional Engine	Information	0.50
G. Operational Interruptions	Information	0.50
	TOTAL THROUGHPUT:	0.00117

Integration time increased by 1/throughput = 853.

Observation Time Calculations

- Total Observation = Integration Time for Ideal System
  $\times$
  Time Factor for Light and Information Losses (853)
  $\times$
  Time Factor for Random Errors (1.36)

- For ATF: Overall Time Factor = $853 \times 1.36 = 1160$

  Observation Time = $1160\times$ Ideal Integration Time

Table I continued.

Quasars	RA h	RA m	RA s	Dec °	Dec '	Dec "	z	m	M	B-V	U-B	Observing Time Ideal(s)	Observing Time Total(h)	REMARK	h	m	s	°	'	"	m	Remark
PKS 1921-293	19	24	50.71	-29	14	30.89		15.40				1508	485.9	Hipp	19	25	27.20	-29	4	55.13	10.98	Hipp
4C 74.26	20	42	36.93	75	9	13.80	.1040	16.40	28.4	.00	.00	1508	485.9		20	43	38.01	75	4	57.86	12.43	
															20	43	58.53	75	13	38.14	11.07	
															20	43	40.78	75	7	53.18	11.40	
															20	42	1.37	75	42	7.30	11.63	
															20	43	14.65	75	13	28.31	10.61	
															20	42	56.03	75	9	43.02	14.60	
4C 73.18	19	27	48.41	73	58	1.60	.3020	15.50	26.8	.00	.00	1653	532.9	Hipp	19	28	45.69	73	57	25.33	12.12	
															19	27	0.11	73	55	47.00	10.37	Hipp
															19	27	51.35	73	50	35.84	12.87	
															19	28	59.40	73	54	40.83	10.64	Hipp
S4 0248+43	2	51	34.48	43	15	15.9	.3160	15.50	29.7	.00	.00	1653	532.9		2	51	36.18	43	10	43.90	12.62	
															2	51	9.36	43	18	27.36	12.12	

Epoch 2000

TABLE II

Data source: (2) and (3)

Object	Name	RA h	RA m	RA s	Dec °	Dec '	Dec "	m	Hipparcos star	RA h	RA m	RA s	Dec °	Dec '	Dec "	m
NGC 7009	Saturn Nebulae	21	4	12	-11	22	00	11.5		21	31	35.0	-11	56	17.1	6.0
PKS 2128-123		21	31	35.3	-12	07	04	16.0								
NGC 2632	Praesepe	8	40	06	19	59		3.1		8	54	31.3	19	57	13.4	10.6
PKS 0851+202		8	54	48.6	20	6	31.2	14.0								
NGC 1039	M 34	2	42	r	42	47		5.2								
S4 0248+43		2	51	34.5	43	15	15.9	15.5								

LEAD EDGE

Data source : (1) Dr. B Mills and Dr. D Wills
(2) Hipparcos (indicated by Hipp)
(3). Sky Catalogue 2000.0 vol 2 , editors: A Hirshfeld & R W Sinnott, Cambridge Univ Press, Cambridge, 1985

NATIONAL 42-385

TABLE I.1

Epoch: 2000

Quasars	RA			Dec			z	m	M	B-V	U-B	Observing Time		REMARK			Reference stars RA			Dec			m	Remark	
	h	m	s	°	'	"						Ideal(s)	Total(h)				h	m	s	°	'	"			
4U241+61	2	44	57.56	62	28	6.10	.0440	12.19	26.8	-.04	-.82	78	25.13	XS1		Hipp	2	45	18.89	62	29	59.78	12.65		
																	2	44	30.36	62	26	55.21	12.18	Hipp	
																	2	44	38.25	62	23	29.04	11.00		
3C 273	12	29	6.58	2	3	8.36	.1580	12.80	26.6	.21	-.85	137	44.38	XS1 J	Var	Hipp	12	29	6.65	2	3	8.24	12.27		
																	12	29	22.22	1	58	39.47	10.70		
																	12	29	3.18	2	3	18.22	12.90		
PKS 2005-489	20	9	24.70	-48	49	53.55		13.36 13.89				262	44.45		var	Hipp	20	9	7.10	-48	55	35.26	10.68	Hipp	
																	20	9	23.25	-48	52	30.83	10.13		
PKS 0851+202	8	54	48.90	20	06	32.0	.3060	14.00		.39	-.64	414	139.70	BL Lac	var		8	54	48.89	20	6	30.10	14.06		
																	8	54	54.45	20	6	13.14	14.61		
																	8	54	29.48	20	10	55.42	11.36		
PKS 0716+714	7	21	53.28	71	20	36.18		13.2 15.5				547	176.5		var	Hipp	7	20	1.76	71	15	17.42	8.27	Hipp	
																	7	20	3.65	71	20	47.08	9.74		
4C 39.49	16	53	52.20	39	45	37.0	.0340	13.88		.72	-.28	346	111.50	BL Lac	var		16	47	35.00	39	26	44.00	7.9		
																	17	00	05.30	39	06	02.00	7.2		
PKS 0754+394	7	57	59.90	39	20	27.0	.0960	14.36		.38	-.71	581	187.21				7	58	0.13	39	20	29.76	13.97		
																	7	57	51.91	39	21	32.40	16.01		
																	7	58	10.93	39	19	42.85	12.53		
PKS 0405-12	4	7	48.41	-12	11	36.31	.5740	14.57	28.5	.18	-.60	702	226.32	S1		Hipp	4	8	6.17	-12	9	6.12	11.92	Hipp	
																	4	7	53.15	-12	9	36.61	12.10		
																	4	7	37.32	-12	12	31.40	12.48		
4C 29.45	11	59	32.20	29	14	45.00	.7200	14.41 15.60	27.2	.39	-.50	606	195.29		var		11	59	45.4	29	14	43.55	14.99		
																	11	59	18.47	29	15	12.56	13.96		
																	11	59	18.04	29	15	15.16	13.76		
PKS 0537-440	05	38	49.75	-44	5	9.33		14.48 16.2				1375	443.2		blazer	Hipp	5	39	4.49	-44	6	38.41	10.99	Hipp	27.7 years period of outburst next year 2000.
																	5	38	13.00	-44	5	25.37	8.80		
PKS 1004+12	10	7	26.10	12	48	56.20	.2400	15.15	28.5	.13	-.82	1198	386.65				10	7	26.10	12	48	55.98	15.01		
																	10	7	13.15	12	44	22.78	13.44		
																	10	7	23.20	12	44	53.81	14.27		
PKS 1302-102	13	5	32.89	-10	33	10.90	.2860	15.23	27.2	-.05	-.82	1290	415.63			Hipp	13	5	41.69	-10	30	6.95	9.97	Hipp	
																	13	5	20.18	-10	36	31.32	12.71		
																	13	5	32.98	-10	33	20.27	14.85		
3C 351.0	17	4	41.38	60	44	28.20	.3710	15.28	28.9	.13	-.75	1350	435.00				17	4	41.57	60	44	28.50	14.57		
																	17	4	48.66	60	47	12.05	10.83		
																	17	5	9.24	60	44	34.62	11.84		
PKS 2349-01	23	51	56.05	-1	9	13.80	.1730	15.33	26.4	.12	-.90	1414	455.65				23	51	56.03	-1	9	13.68	15.55		
PKS 0430+052	4	33	10.43	5	21	16.98		15.30				1315	443.2			Hipp	4	33	50.50	5	23	10.43	7.94	Hipp	
																	4	32	37.46	5	27	22.54	10.14		
																	4	33	16.93	5	29	35.09	10.78		

LEAD EDGE